Subseasonal-to-seasonal predictability of the Southern Hemisphere eddy-driven jet during austral spring and early summer

Article

Accepted Version

It is advisable to refer to the publisher's version if you intend to cite from the work. See Guidance on citing.

www.reading.ac.uk/centaur

Subseasonal-to-seasonal predictability of the Southern Hemisphere eddy-driven jet during austral spring and early summer

Nicholas J. Byrne[1][*] **, Theodore G. Shepherd**[1]**, Inna Polichtchouk**[2]

[1]Department of Meteorology, University of Reading, Reading, United Kingdom

[2]European Centre for Medium-Range Weather Forecasts, Reading, United Kingdom

Key Points:

- SH midlatitude jet variations in spring and early summer are predictable several months ahead
- This subseasonal-to-seasonal predictability of the SH jet comes via the stratospheric polar vortex
- The observed influence of ENSO on the jet during this time is via this stratospheric pathway

[*]Present affiliation: European Centre for Medium-Range Weather Forecasts, Reading, UK

Corresponding author: Nicholas Byrne, `n.byrne@ecmwf.int`

Abstract

Several recent studies have suggested that the stratosphere can be a source of subseasonal-to-seasonal predictability of Southern Hemisphere circulation during the austral spring and early summer seasons, through its influence on the eddy-driven jet. We exploit the large sample size afforded by the hindcasts from the European Centre for Medium-Range Weather Forecasts Integrated Forecast System to address a number of unanswered questions. It is shown that the picture of coherent seasonal variability of the coupled stratosphere-troposphere system apparent from the reanalysis record during the spring/early summer period is robust to sampling uncertainty, and that there is evidence of nonlinearity in the case of the most extreme variations. The effect of El Niño-Southern Oscillation on the eddy-driven jet during this time of year is found to occur via the stratosphere, with no evidence of a direct tropospheric pathway. A simple two-state statistical model of the stratospheric vortex is introduced to estimate the subseasonal-to-seasonal predictability associated with shifts of the seasonal cycle in the SH extratropical atmosphere. This simple model, along with a more general model, are subsequently used to interpret skill scores associated with hindcasts made using the full seasonal forecast model. Together the results provide evidence of tropospheric predictability on subseasonal-to-seasonal timescales from at least as early as August 1, and show no evidence of a 'signal-to-noise paradox' between the full seasonal forecast model and the reanalysis.

1 Introduction

Subseasonal-to-seasonal (S2S) forecasts for the extratropical troposphere are regularly regarded in a statistically heterogeneous manner; they are viewed as being most skilful during specific 'windows of opportunity' [*WMO*, 2013]. In this context, the influence of the stratosphere has received considerable attention in recent years. In the Northern Hemisphere (NH), winter is a period of particular focus. This is due to the occurrence of large perturbations to the stratospheric polar vortex (SPV), referred to as stratospheric sudden warmings (SSW), during the winter season. SSWs typically precede an equatorward shift of the tropospheric eddy-driven jet [EDJ; *Baldwin and Dunkerton*, 2001; *Hitchcock and Simpson*, 2014], and forecasts initialised during SSWs have been found to yield greater S2S forecast skill in the troposphere (in specific regions) than those that are not [*Sigmond et al.*, 2013]. In the Southern Hemisphere (SH) SSWs are much rarer events [*Roscoe et al.*, 2005], and interest has instead focused on the period in the lead-

up to the annual SPV breakdown event, which generally occurs sometime in late spring/early summer [*Black and McDaniel*, 2007]. The strength of the SPV during this lead-up period has a strong influence on the timing of the breakdown event, as well as on the latitude of the EDJ in the troposphere [*Byrne and Shepherd*, 2018]. In addition, the SPV breakdown event itself typically precedes an equatorward shift of the EDJ [*Byrne et al.*, 2017]. This close relationship between the SPV and the EDJ in the SH can be parsimoniously viewed as a continuous shift of the seasonal cycle during this time of year [*Byrne and Shepherd*, 2018]. This perspective suggests the potential for extended predictability in the extratropical SH troposphere during austral spring and summer, with the important caveat that there may be considerable sampling uncertainty associated with the magnitude of the predictable signal [*Kumar*, 2009]. Evidence for extended-range predictability during this time of year has been realised in a number of recent modelling studies [*Roff et al.*, 2011; *Son et al.*, 2013; *Lim et al.*, 2013; *Seviour et al.*, 2014], although most of these studies only considered sub-intervals of the entire spring/summer period and/or the observational record.

The phase of El Niño-Southern Oscillation (ENSO) offers another opportunity for extended range forecasts of the extratropical troposphere. In the SH, the observed extratropical response to ENSO shifts from a zonally asymmetric pattern in spring to a more zonally symmetric pattern in summer. This zonally symmetric pattern has been viewed as a forced response to ENSO via a direct tropospheric pathway [*Seager et al.*, 2003; *L'Heureux and Thompson*, 2006; *Lim et al.*, 2013]. However, the troposphere is not the only potential pathway for such remote extratropical impacts; the stratosphere provides another possible pathway. Work over recent decades has much improved the understanding of the relevant mechanisms for this stratospheric pathway [*Domeisen et al.*, 2019]. Indeed, in regions such as the North Atlantic, impacts via the stratosphere are able to completely overwhelm any potential impacts via the troposphere [*Polvani et al.*, 2017]. In the SH, the extratropical stratospheric pathway for ENSO is most prominent during austral spring and summer, a similar time period as for the observed zonally symmetric response to ENSO (*Hurwitz et al.* [2011]; *Lin et al.* [2012]; *Zubiaurre and Calvo* [2012]; see also *Domeisen et al.* [2019]). This poses the challenge of how best to separate the impacts of these two pathways, especially given the limited observational record. *Byrne et al.* [2017] attempted this separation in observations via a regression-based approach and concluded that the stratospheric pathway was dominant. More recent work

by *Vera and Osman* [2018], who showed that the 'failed' zonally symmetric response to the large El Niño of 2015/2016 was consistent with an exceptionally strong SPV, also supports this conclusion.

In this paper we address these specific issues of S2S predictability and sampling variability for the SH extratropical atmosphere during the spring and summer period by analysing a large ensemble of seasonal forecast model data. We begin by using the ensemble to explore the impact of sampling uncertainty on some previous statistical results in the literature. We then use the ensemble to develop a simple statistical model for estimating the S2S predictability associated with shifts of the seasonal cycle in the SH extratropical troposphere. We subsequently use this simple model, along with the statistical model of *Kumar* [2009], to interpret skill scores associated with hindcasts made using the full seasonal forecast model. This includes investigation of whether there is any evidence of a mismatch between anomaly correlation and signal-to-noise ratio - known as the 'signal-to-noise paradox' [*Scaife and Smith*, 2018]. We conclude with a summary of our results.

2 Data and Methods

We use ECMWF System 4 hindcast data [*Molteni et al.*, 2011]. System 4 is based on the IFS atmospheric component coupled to the NEMO ocean model. The atmospheric resolution is T255L91, which corresponds to approximately 80 km horizontally with 91 levels in the vertical. The resolution of the ocean model is 1 degree in the horizontal and has 42 layers in the vertical. All hindcasts are issued as ensembles with 51 members. The hindcast data is available over the period 1981-2016. Here we consider hindcasts initialised on August 1 and November 1 as these are the relevant dates for the period of austral spring and austral summer.

For verification we use the ERA-Interim reanalysis [*Dee et al.*, 2011]. The basic data input for our study is daily-mean zonal wind and geopotential data for the period 1 August 1981 to 31 January 2016, which encompasses 35 years in total. Data were available on a N128 Gaussian grid. Before analyzing the data, we first processed them by forming a zonal average. We denote this zonal average for the remainder of the paper using the [.] notation. We use zonally-averaged zonal wind ([u]) at 850hPa as a measure of the eddy-driven jet. We define a daily jet latitude index by computing the latitude of the

110 maximum value of [u] between 35S and 70S at 850hPa; no interpolation is used. We iden-

111 tify the date of the stratospheric vortex breakdown as the final time that [u] at 60S drops

112 below 10 m/s; we apply this criterion to running 5-day averages at 50 hPa [*Black and*

113 *McDaniel*, 2007]. We define an index of interannual stratospheric variability as the lead-

114 ing principal component time series that emerges from a multiple empirical orthogonal

115 function analysis on monthly-mean polar cap-averaged (60S - 90S) geopotential height

116 at 50hPa, following *Byrne and Shepherd* [2018]. This method proceeds by combining X

117 successive months of data in a vector for a given year, and then repeating this for all years.

118 Each eigenvector will then have X elements. Here, we set X=6, so as to span the entire

119 austral spring and summer period. We define an ENSO index by averaging sea-surface

120 temperatures across the Niño 3.4 region (5N-5S, 170W-120W). We define El Niño years

121 as those years in the upper quartile of this index (i.e., the warmest 25% of years) and

122 La Niña years as those years in the lower quartile (i.e., the coldest 25% of years). We

123 examine the sea ice evolution using monthly-mean sea ice extent data from the U.S. Na-

124 tional Snow and Ice Data Center (www.nsidc.org).

3 Role of Sampling Uncertainty

126 We begin by comparing the large-scale extratropical circulation during austral spring

127 and summer in the hindcasts and in ERA-Interim. The purpose of this is two-fold. Firstly,

128 we wish to confirm that the hindcasts have realistic circulation statistics. Secondly, once

129 that is confirmed, the large hindcast ensemble size allows us to explore the potential im-

130 pact of sampling uncertainty on the reanalysis results, to determine their robustness as

131 well as to explore possible nonlinearities. Thus, the comparison between hindcasts and

132 observations works in both directions. In most of what follows we exclude the year of

133 2002 from our analysis. The only SSW in the SH in the observational record occurred

134 in 2002 [*Roscoe et al.*, 2005], an event which was notable for its extreme impacts in both

135 the stratosphere and troposphere [*Thompson et al.*, 2005]. We exclude 2002 so that our

136 results are not unduly reliant on such an extreme event.

3.1 The eddy-driven jet

153 Figure 1a shows the long-term average for the EDJ in ERA-Interim and Figure 1b

154 shows a similar quantity for the hindcasts, based on initialisations on August 1. The semi-

155 annual oscillation [SAO; *van Loon*, 1967] in the latitude of the EDJ is visible in both pan-
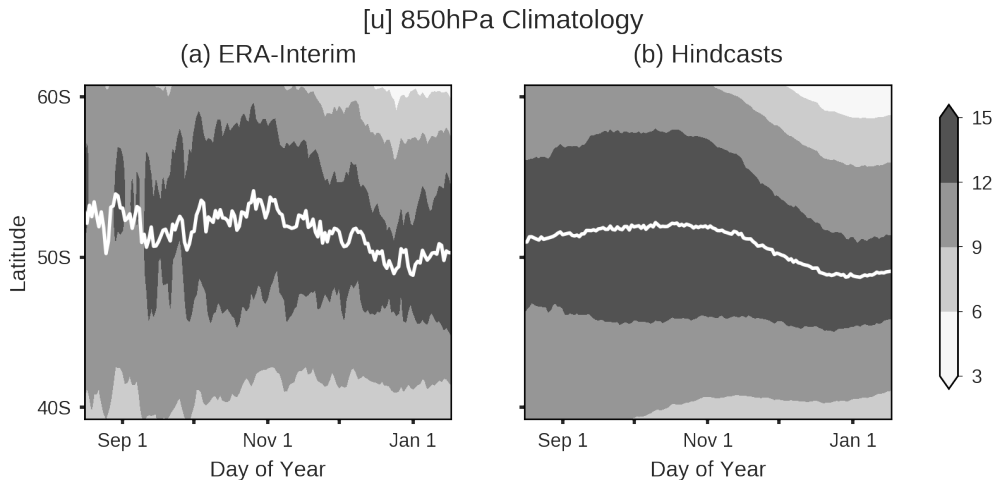
[u] 850hPa Climatology

Figure 1. (a) Climatology of [u] 850hPa (m/s, shading) and jet-latitude index (white line) for ERA-Interim, 1981 - 2015. The year of 2002 has been excluded. (b) Similar, but for the entire hindcast ensemble based on August 1 initialisations.

els from about October onwards, with the EDJ seen to be closer to the pole in spring and closer to the equator in summer. The impact of sampling uncertainty is visible in the 'noisy' appearance of the ERA-Interim average, and also in the relatively large confidence intervals for such averages during spring and early summer (Figure 2). There is a suggestion of an equatorward model bias developing several months into the hindcast, with this bias becoming gradually more noticeable as the summer months progress. However, even six months after the model initialisation, the magnitude of this potential bias is still within the sampling uncertainty (Figure 2). The hindcasts also appear to mimic observed variability in the EDJ, with a noticeable seasonal decrease in the variability of the latitude of the EDJ in both the hindcasts and the observations (Figure 3). Figure 4 provides a broader assessment of model zonal-wind bias for the August 1 initialisations. Broadly speaking, outside of the tropics and some very high-latitude regions during the month of September, there appears to be good agreement between the hindcasts and ERA-Interim in the stratosphere. In the troposphere, an equatorward bias in the EDJ is seen to emerge from about December onwards, consistent with what was noted for Figure 2.
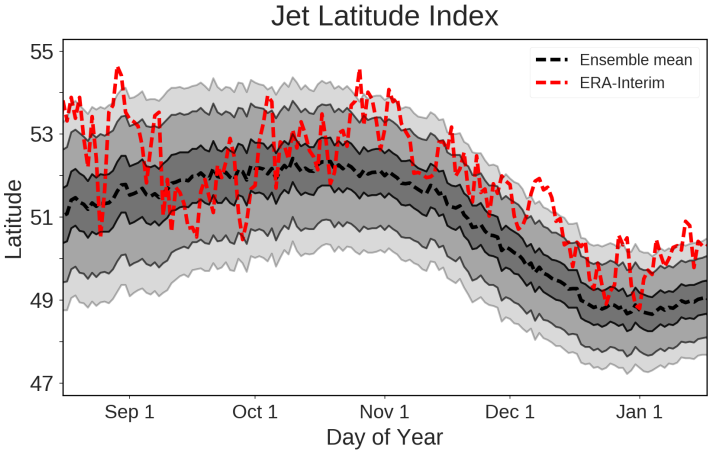
Figure 2. Bootstrap estimate of sampling uncertainty associated with 34-year mean of jet latitude using ensemble members from the August 1 initialisations. The bootstrap estimate was generated using 10000 time series of length 34 where an ensemble member has been randomly selected from each year in the 34-year period excluding the year of 2002. Solid lines represent 1, 5, 25, 75, 95 and 99% thresholds respectively. Dashed red line indicates jet latitude from ERA-Interim.
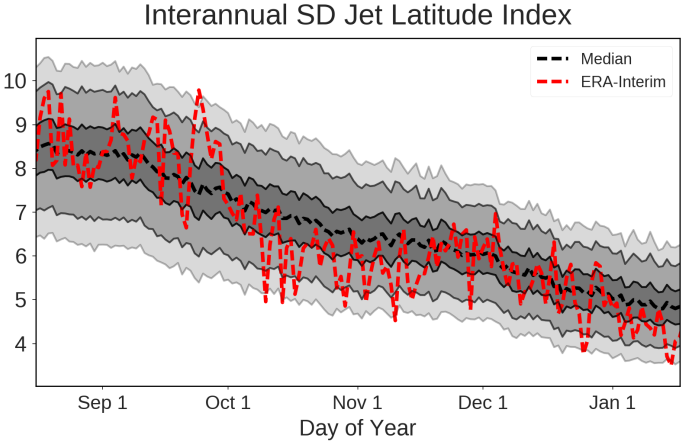
Figure 3. Similar to Figure 2, except using standard deviation instead of mean.
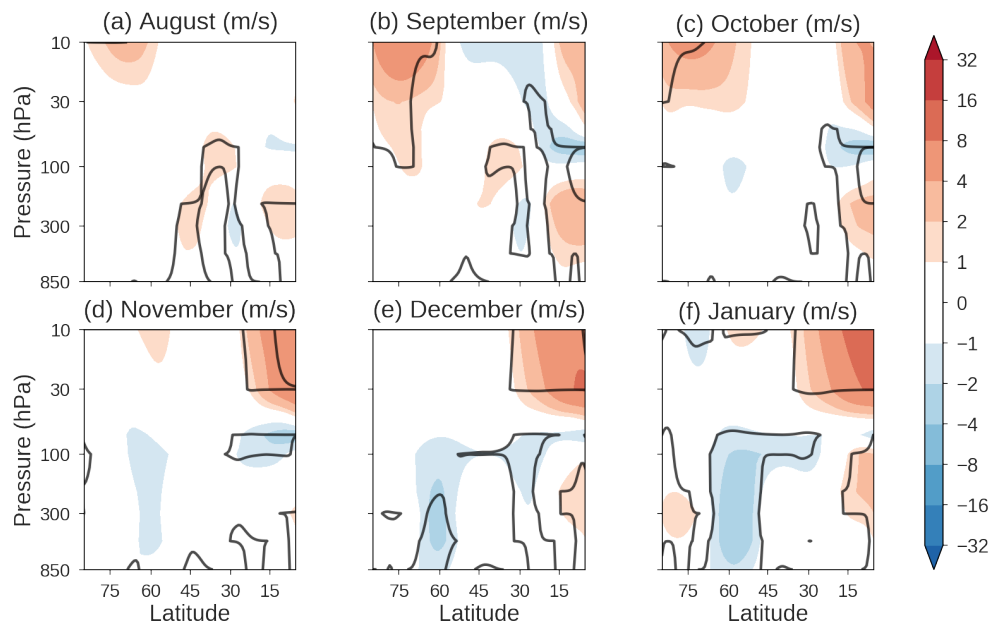
Figure 4. Monthly-mean climatological differences in [u] between hindcasts and ERA-Interim (m/s, shading) for (a) August, (b) September, (c) October, (d) November, (e) December and (f) January, 1981-2015. The year of 2002 has been excluded. Black contours indicate differences that are statistically different at the 1% level based on a two-sided two-sample t-test. Hindcasts initialised on August 1.
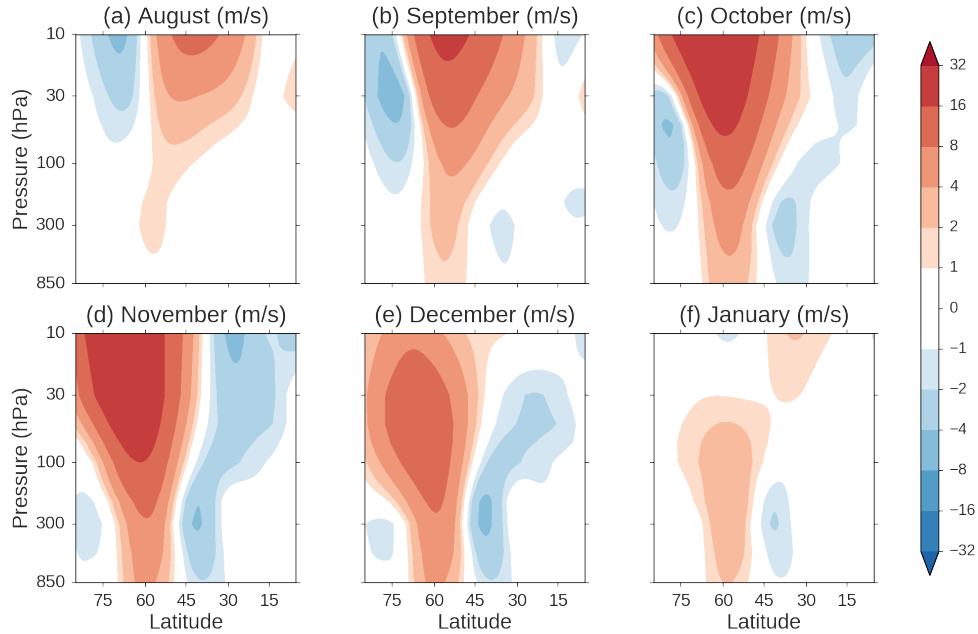
Figure 5. Monthly mean differences in [u] between upper and lower quartiles of the hindcast ensemble for August 1 initialisations, based on an index of stratospheric variability (see text for details). Please note that Figure 5 from *Byrne and Shepherd* [2018] represents the difference between upper and lower halves of the data, rather than the upper and lower quartiles used here, because of the limited sample size of the observational record. The difference between the upper and lower halves of the data for the hindcast ensemble is included in the Supplementary Material. Please also note the nonlinear color scale that is required for including tropospheric and stratospheric differences in the same figure. The year of 2002 has been excluded from all calculations.

This equatorward bias in December and January is not present in hindcasts initialised on November 1 (see Supplementary Material). To confirm that our results are not unduly sensitive to model bias, we verify that all results obtained for December and January are robust to the choice of initialisation date.

Next, we move on to considering coupled variability between the SPV and the EDJ. Figure 5 represents an estimate of this variability using the hindcast ensemble. It was constructed in a similar manner to previous reanalysis-based results ([*Byrne and Shepherd*, 2018]; see also *Hio and Yoden* [2005]). Briefly, an index of interannual variability in the extratropical stratosphere was applied to individual years in the ensemble. This

189 index was then used to stratify the ensemble into quartiles, and to produce a compos-

190 ite difference between the lower and upper quartiles. The coupled patterns that are ev-

191 ident in Figure 5 can be parsimoniously viewed as a continuous shift of the seasonal cy-

192 cle in the stratosphere and the troposphere during this time of year [*Byrne and Shep-*

193 *herd*, 2018]. During years where the stratospheric seasonal cycle is delayed in spring, there

194 tends to be a corresponding delay in the timing of the SPV breakdown event in early

195 summer; such years also tend to be associated with a stronger poleward shift of the EDJ

196 between September-November and with a delay in the equatorward shift of the EDJ in

197 early summer. The converse behaviour is found to occur on average in years with an ac-

198 celerated stratospheric seasonal evolution in spring. The patterns of coupled stratosphere-

199 troposphere variability seen in Figure 5 are very similar to those found for reanalyses ([*Byrne*

200 *and Shepherd*, 2018]; see also *Hio and Yoden* [2005]). The large ensemble size used here

201 ensures a high degree of statistical confidence in all plotted differences, indicating that

202 previous reanalysis-based results using 38 years of data are qualitatively robust to sam-

203 pling variations.

212 Figure 6 focuses on the equatorward transition of the EDJ in early summer using

213 hindcasts initialised on November 1, so that the hindcasts are as close to observations

214 as possible during the vortex breakdown period. The timing of the equatorward tran-

215 sition of the EDJ has been found to be closely coupled to the SPV breakdown date in

216 the reanalysis [*Byrne et al.*, 2017]. In particular, years with a later than average SPV

217 breakdown date are associated with a later than average equatorward transition of the

218 EDJ, with opposite behaviour for earlier than average years. To test the robustness of

219 this relationship to sampling variability, we first define an index for the SPV breakdown

220 date [*Black and McDaniel*, 2007] and apply this index to all years in the ensemble. We

221 then divide the ensemble into late (L; upper half) and early (E; lower half) and plot daily

222 averages of the EDJ (Figures 6a and 6b); both late and early sets contain approximately

223 900 breakdown events. These figures confirm what was previously found for the reanal-

224 ysis: earlier SPV breakdown years are seen to have an earlier equatorward transition of

225 the EDJ, with opposite behaviour in late SPV breakdown years. This behaviour can be

226 seen most clearly in Figure 6c, where the difference between late and early years is shown.

227 We can also exploit the large ensemble size to explore the extremes of the system

228 behaviour. One motivation for studying circulation extremes at this time of year is that

229 they may be relevant for reducing the uncertainty in the ozone-hole-induced tropospheric
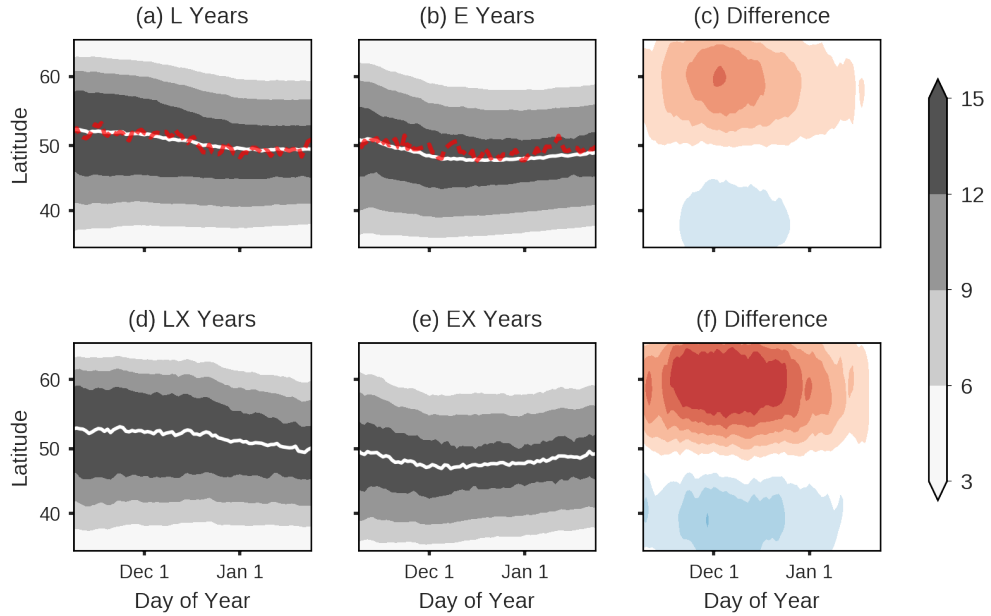
Figure 6. Average of [u] 850hPa (m/s, shading) and jet-latitude index (white line) for (a) upper half (late), (b) lower half (early), (d) upper decile (extreme late) and (e) lower decile (extreme early) of SPV breakdown years in hindcast ensemble (see text for further details). Panel (c) shows difference between (a) and (b) and panel (f) shows difference between (d) and (e). The contour interval in (c) and (f) is 1 m/s, with values between -1 and 1 m/s set to white. The red dashed line indicates jet-latitude index for (a) upper half (late) and (b) lower half (early) of SPV breakdown years from ERA-Interim (see also *Byrne et al.* [2017]). The year of 2002 has been excluded from all calculations.

230 circulation changes [see *Son et al.*, 2018, and references therein]. Here we define extreme

231 late (LX) and early (EX) SPV breakdown years as upper and lower deciles of the data

232 (Figure 6d and Figure 6e). There is a qualitative similarity in the behaviour between L

233 and LX years, and similarly for E and EX years, with the timing of the equatorward tran-

234 sition of the EDJ seen to shift with the timing of the SPV breakdown date. However,

235 it is also clear that this transition appears to proceed substantially less equatorward in

236 LX years compared to EX years, with the result that perturbations to EDJ latitude ap-

237 pear to persist well into January in LX years (Figure 6f). Thus, a model of circulation

238 variability that accounts for both a shift in timing and change in amplitude of the EDJ

239 transition would appear most appropriate for characterising long-term changes. Such a

240 model was previously proposed by *Sun et al.* [2014] as an explanation for the recent trends

241 in the troposphere and stratosphere; the results of the hindcast ensemble used here would

242 appear to lend further support to this hypothesis.

3.2 ENSO

244 The observed zonally symmetric extratropical summertime response to ENSO is

245 characterised as a shift in latitude of the EDJ [*Seager et al.*, 2003; *L'Heureux and Thomp-*

246 *son*, 2006; *Lim et al.*, 2013]. One complication in using a reanalysis to quantify the mag-

247 nitude of this effect is that the limited observational record makes it difficult to control

248 for potentially confounding effects such as the SPV, i.e. to distinguish between tropo-

249 spheric and stratospheric pathways. Here we try to overcome this difficulty by exploit-

250 ing the large ensemble size. Formally, given a variable X (EDJ) that is potentially re-

251 sponsive to variables Y (ENSO) and Z (SPV), we consider the difference in X between

252 two extremes of Y while holding Z fixed, and similarly for extremes of Z while holding

253 Y fixed.

263 To begin, we address the reverse question of whether the influence of the SPV on

264 the EDJ might be confounded by the influence of ENSO. To do this, we perform a sim-

265 ilar analysis to Figure 5 but only allowing years where an El Niño event was simulated

266 in the hindcasts i.e., we condition on El Niño events (Figure 7). The results are virtu-

267 ally identical to Figure 5. This shows that the results from the previous section are ro-

268 bust to potentially confounding effects from ENSO. We now proceed to explore the EDJ

269 response to ENSO in the hindcast ensemble. Figure 8 shows the El Niño minus La Niña

270 response for hindcasts initialised on August 1. Consistent with the previously mentioned
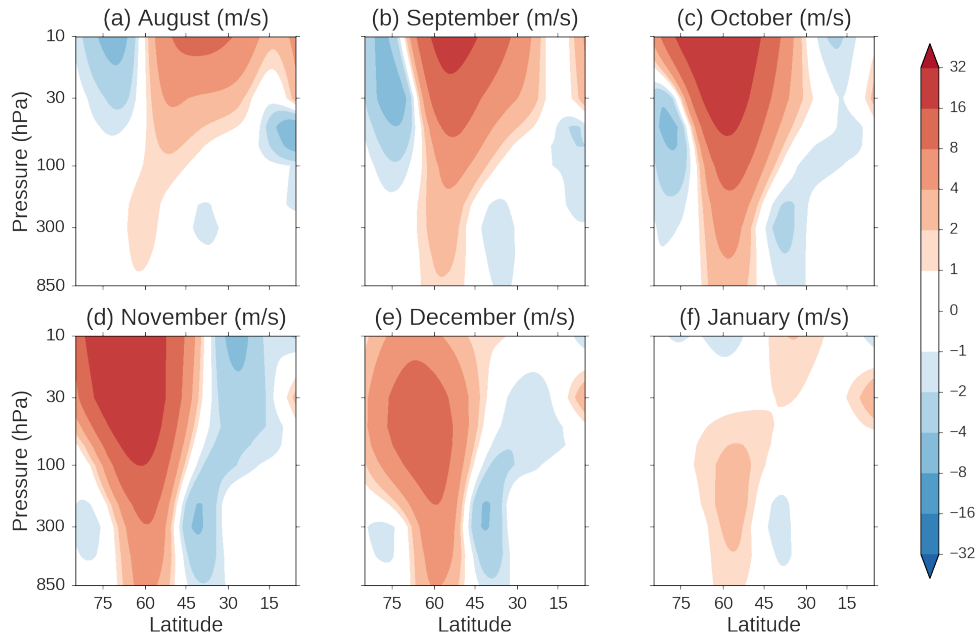
Figure 7. Similar to Figure 5, but conditioned on El Niño events (see text for details). The year of 2002 has been excluded from all calculations. See Supplementary Material for differences conditioned on La Niña events.
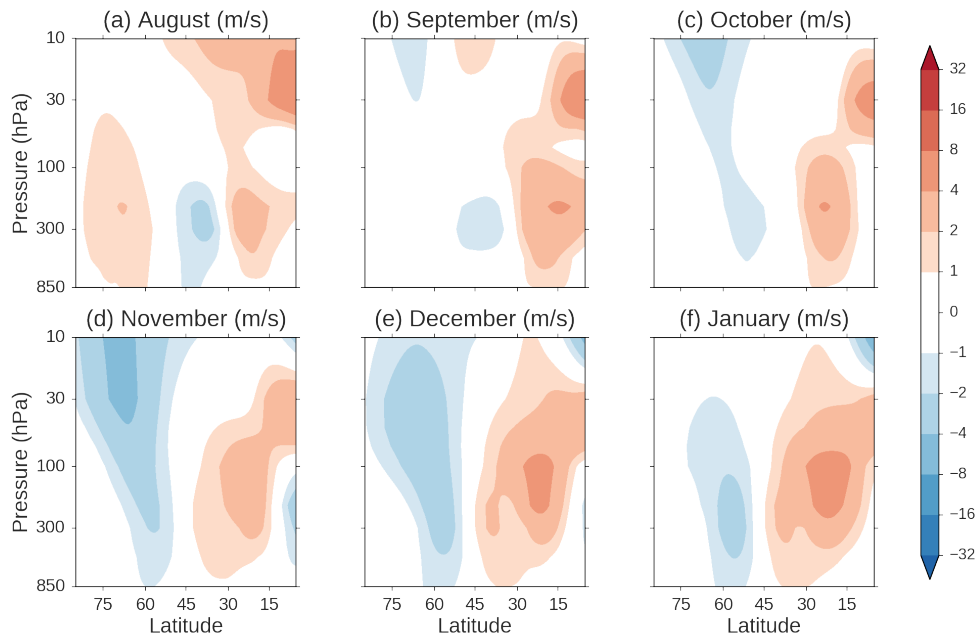
Figure 8. Monthly-mean differences in [u] between El Niño and La Niña years for August 1 initialisation (see text for details). The year of 2002 has been excluded from all calculations.
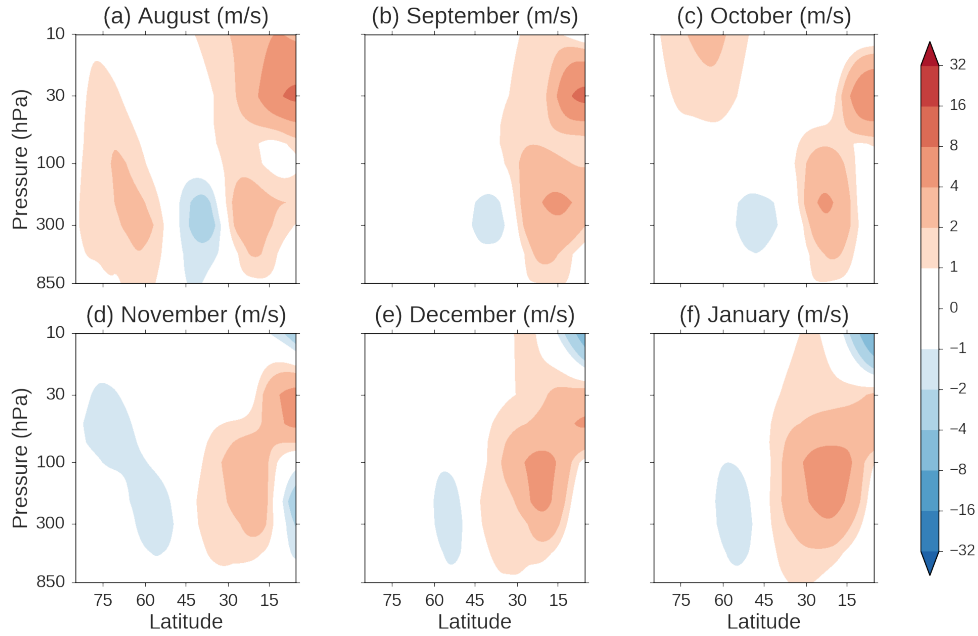
Figure 9. Similar to Figure 8, but conditioned on lower quartile of stratospheric variability

260 index (see text for details). The year of 2002 has been excluded from all calculations. See Sup-

261 plementary Material for differences conditioned on upper quartile of stratospheric variability

262 index.

271 results for the reanalysis, an EDJ response is seen to emerge from about November on-

272 wards. However, this figure also contains evidence of an SPV response to ENSO that pre-

273 cedes the EDJ response in time. This suggests that the SPV may be acting as a confound-

274 ing variable or, equivalently, that any potential ENSO-EDJ link is via a stratospheric

275 pathway. To test this hypothesis, we repeat our analysis using only years from the lower

276 quartile of our stratospheric variability index i.e., we condition on the SPV (Figure 9).

277 The large reduction in the EDJ response in this figure is consistent with our hypothe-

278 sis of a stratospheric pathway for the ENSO-EDJ influence, in that the influence is markedly

279 reduced when the stratospheric pathway is blocked by conditioning on the SPV.

285 As a complementary approach to this conditional analysis, we also perform a regression-

286 based analysis similar to that described in *L'Heureux and Thompson* [2006] and *Byrne*

287 *et al.* [2017]. Briefly, monthly-mean [u] at 850hPa and averaged over 55-65S is correlated

288 against an index for ENSO for November, December and January separately. This anal-

289 ysis is then repeated after first linearly regressing out the impact from the SPV (see *Byrne*

Month	ERA	ERA - No SPV	Hindcasts	Hindcasts - No SPV
Nov	0.26	0.14	0.14 (-0.14, 0.40)	0.08 (-0.21, 0.35)
Dec	**0.33**	0.14	0.19 (-0.08, 0.44)	0.07 (-0.20, 0.34)
Jan	0.16	0.01	0.24 (-0.03, 0.48)	0.03 (-0.24, 0.29)

Table 1.   Correlation between 850hPa [u] averaged over 55-65S and ENSO, for ERA-Interim and for hindcasts based on August 1 initialisation, with and without the influence from the SPV. Hindcast columns show median value along with 5 and 95% confidence intervals. See text for further details. Bold values indicate quantities that are statistically different from zero at the 5% level based on a one-sided two-sample t-test.

et al. [2017] for further details). The results from ERA-Interim are shown in Table 1. They indicate that the correlation between ENSO and EDJ is relatively weak, and that it is further reduced once the stratospheric pathway has been removed. To compare these observational results against the hindcasts, we begin by generating a synthetic time series of length 34 by randomly selecting an ensemble member from each year (excluding 2002) for hindcasts initialised on August 1. We then repeat the above correlation analysis for this synthetic time series. We do this for 10000 synthetic time series to generate a distribution. The results are again shown in Table 1. Firstly, it is clear that all values from observations lie within the 5 and 95% confidence intervals for the hindcasts. This indicates that any differences in the correlations between the observations and the hindcasts are consistent with sampling variability. Secondly, the results from the hindcasts indicate that any correlation between ENSO and EDJ essentially vanishes once the stratospheric pathway has been controlled for. Thus, combining these results with the previous results from the conditional analysis, we conclude that there is a close relationship between the SPV and EDJ throughout austral spring and summer, and this relationship means that the SPV has the potential to act as a confounding variable unless suitably controlled for. It should be noted that although our results suggest that any tropospheric ENSO-EDJ pathway is weak through spring and early summer, they do not preclude the existence of a tropospheric pathway following the breakdown of the SPV. Further research is required to establish the robustness of any such pathway.

4 S2S Hindcasts of the Extratropical Circulation

In the previous section a robust relationship was established between perturbations to the seasonal cycle of the SPV and the seasonal cycle of the EDJ from August until January. In addition, evidence was presented that any potential relationship between ENSO and the EDJ during this time period was also likely via (perturbations to the seasonal cycle of) the SPV. A natural question that emerges from these results is whether such shifts of the seasonal cycle are predictable on S2S timescales, and if so, whether they might allow skilful forecasts of the EDJ on S2S timescales?

To begin to answer this question, firstly we note that several previous studies have highlighted that the SH SPV exhibits long autocorrelation timescales from August until December [see *Gerber et al.*, 2010, and references therein]. These long timescales can be viewed as evidence for the predictability of shifts of the seasonal cycle of the SPV. Indeed, such predictability has been found for hindcasts from August 1 in a previous study [*Seviour et al.*, 2014]. We reach similar conclusions for the hindcasts from August 1 that are used in this study by computing receiver operating characteristic (ROC) curves for early, late, extreme early and extreme late years for the SPV in observations (Figure 10). Here we have repeated our analysis from the previous section and classified each year from the observations as early, late, extreme early or extreme late depending on whether it is contained in the lower or upper halves or quartiles of the index of interannual stratospheric variability in observations. The ROC curves indicate that the model appears able to predict shifts of the seasonal cycle based on an August 1 initialisation, with a suggestion of greater forecast skill for years with a more extreme shift of the seasonal cycle.

Given these apparently predictable shifts of the seasonal cycle of the SPV, we now explore the implications for S2S forecasts of the EDJ. We do this in three ways. First, we introduce a simplified two-state model in an attempt to better understand the 'signal' and 'noise' characteristics of the full system. We then compare the predictions of this simplified model against those that emerge from a more general model of signal and noise [*Kumar*, 2009]; this model is more general as it permits a continuous rather than a discrete (i.e., two-state) representation of the signal. Finally, we compare both of these results against estimates of skill derived from verifying hindcast data against observations. It is assumed that conclusions that are common to all three methods will not be unduly sensitive to the underlying assumptions for any one particular method.
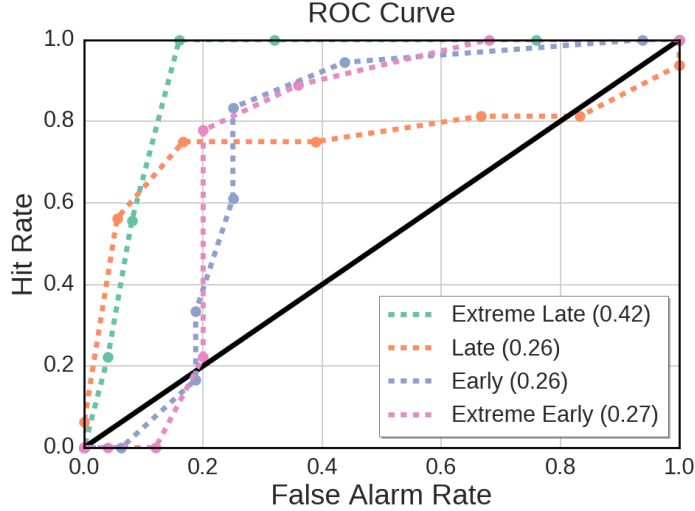
ROC Curve

Figure 10. ROC curves for hindcasts for extreme late, late, early and extreme early strato-
sphere years from ERA-Interim (see text for details on how these years are defined). Values in
brackets indicate area under ROC curves minus area under black diagonal line. The year of 2002
has been excluded from all calculations.

To derive our simplified two-state model we begin by assuming that individual years
can be classified into one of two types, late or early, and that both types occur with equal
probability (here late and early refer to upper and lower halves of the index of strato-
spheric interannual variability). We stress that this is a gross simplification of the ac-
tual system behaviour, where shifts of the seasonal cycle are likely better viewed as a
continuous spectrum rather than as discrete regimes. Next we assume that these two types
of years can be characterised by their means (μ_L, μ_E) and standard deviations (σ_L, σ_E),
and that $\sigma_L = \sigma_E$. We use the large model ensemble to estimate values for all of these
quantities (Figure 11); it should be noted that all of these quantities are a function of
calendar day. Finally, we assume that for each year our model is able to forecast whether
a late or early year will occur, but nothing further. This means that for each individ-
ual year, our ensemble-mean forecast will be $(\frac{\mu_L+\mu_E}{2} \pm \frac{\mu_L-\mu_E}{2})$. For a sufficiently large
ensemble and verification time series, we expect that forecast skill should be a function
of a so-called 'signal-to-noise' ratio $\frac{\mu_L-\mu_E}{2\sigma_L}$ (see Appendix A of *Kumar* [2009] for a deriva-
tion of how this ratio can be related to forecast skill). In what follows we use anomaly
correlation (AC) as our measure of forecast skill; the expected value of AC is equal to
$\frac{s}{(1+s^2)^{0.5}}$, where $s = \frac{\mu_L-\mu_E}{2\sigma_L}$. For later sections it is helpful to remember that, even for
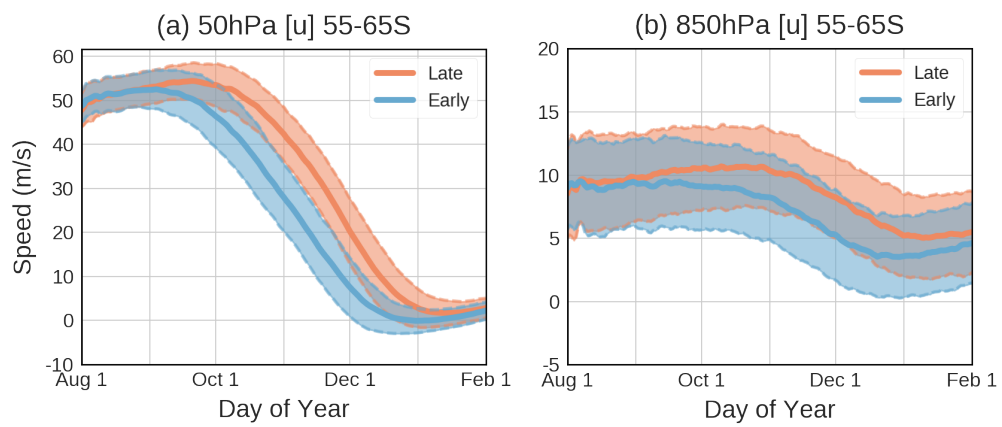
Figure 11. (a) Mean (solid line) and mean plus/minus one standard deviation (dashed lines) for 50hPa [u] 55-65S for late (red) and early (blue) years in hindcast ensemble for August 1 initialisations. (b) Similar, but for 850hPa [u] 55-65S. See text for details on how early and late years are defined. The year of 2002 is excluded from all calculations.
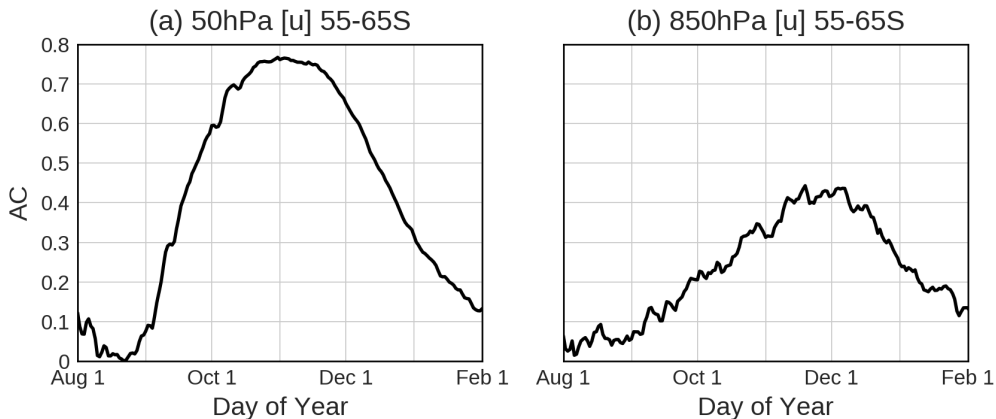
370 **Figure 12.** Expected AC for two-state model for (a) 50hPa [u] 55-65S and (b) 850hPa [u]

371 55-65S.

367 a perfect forecast model, AC values for a given verification time series will still likely dif-

368 fer from this expected AC value due to sampling effects associated with finite ensemble

369 and verification time series length.

372 The expected anomaly correlation for the two-state model is shown in Figure 12.

373 In both the stratosphere and troposphere this value is seen to increase monontonically

374 from about September until November as a result of an increase in the signal during this

375 period (Figure 11). Maximum values in the troposphere emerge during November and

376 are seen to persist into December. These values then rapidly decay from mid-December

377 onwards, following the conclusion of the SPV breakdown event. The results of this sim-

378 ple model suggest that predictable shifts of the SPV seasonal cycle should lead to non-

379 negligible values of S2S forecast skill in the troposphere between mid-October and Jan-

380 uary.

381 We now consider whether there is agreement between the predictions of this two-

382 state model and a more general signal-to-noise model. In this more general model the

383 signal is defined as the interannual standard deviation of the ensemble mean and the noise

384 is defined as the standard deviation of the ensemble members about the ensemble mean.

The advantage of this model over the two-state model is that it allows for a more realistic representation of the signal - it recognises that forecast skill may be larger in years where there is a more extreme shift of the stratospheric seasonal cycle. More specifically, it allows for a continuous rather than a discrete representation of the signal. A potential disadvantage of this alternative signal-to-noise model is that recent work has suggested that some forecast models used in numerical weather prediction may be over-dispersive ([*Scaife and Smith*, 2018]; but see also *Weisheimer et al.* [2019]). If such an over-dispersive scenario was the case for the present hindcast ensemble, then this alternative signal-to-noise model would offer an unduly pessimistic estimate of S2S forecast skill. In particular, if the present hindcast ensemble were to be over-dispersive in its forecasts for shifts of the stratospheric seasonal cycle, then this would likely have a negative impact on estimates of S2S tropospheric forecast skill. In such a scenario, comparison with predictions from the two-state model may be instructive as it only predicts the sign of the shift of the stratospheric seasonal cycle, not its magnitude.

Tropospheric values for signal, noise and expected AC from the more general signal-to-noise model are shown for the hindcasts initialised on August 1 and November 1 in Table 2 and Table 3. We have also included 5 and 95% confidence intervals for the expected AC by employing a bootstrap procedure over the hindcast ensemble; these confidence intervals quantify the sampling uncertainty associated with using finite (i.e. 34-year) verification time series. To first order, the predictions of this more general signal-to-noise model are in agreement with the predictions from the two-state model. In particular, the tropospheric signal is predicted to be largest between November and January in both of the methods and for both August 1 and November 1 initialisations. To further assess the predictions of both of these signal-to-noise models, we compute AC values between ERA-Interim and the ensemble means of hindcasts initialised on both August 1 and November 1 (Figures 13a and 13b). Prior to computing these AC values, we first apply a running-mean to all data. The length of the running-mean used for each figure is motivated by the forecast lead time (31-day and 7-day running means respectively) as this method has previously been suggested as appropriate for verifiying forecasts on S2S timescales [*White et al.*, 2017, see their Figure 1]. The AC values in Figures 13a and 13b are found to agree well with the predictions from both the two-state model and the more general signal-to-noise model, in terms of both amplitude and seasonality. This agreement is particularly striking for the August 1 initialisations, where

Month	Signal (S)	Noise (N)	AC - S/N	AC - ERA	RMSE/Spread	RMSE/SD-ERA
Aug	1.51	1.40	0.73 (0.59, 0.84)	**0.78**	1.36 (0.83, 1.26)	0.66
Sep	0.57	1.86	0.29 (-0.06, 0.49)	-0.12	0.98 (0.81, 1.28)	1.09
Oct	0.59	1.93	0.29 (-0.04, 0.50)	0.23	1.23 (0.83, 1.25)	0.98
Nov	0.77	2.29	0.32 (-0.01, 0.52)	**0.45**	1.39 (0.82, 1.28)	0.90
Dec	0.84	2.37	0.33 (0.02, 0.53)	**0.30**	1.08 (0.83, 1.25)	0.95
Jan	0.70	2.03	0.32 (0.01, 0.52)	**0.28**	1.11 (0.83, 1.25)	0.96

399   **Table 2.**   Values of signal (m/s), noise (m/s), expected AC (along with 5% - 95% confidence

400   interval), ERA-Interim AC, RMSE/Spread (along with 5% - 95% confidence interval) and

401   RMSE/SD(ERA) for monthly-mean [u] 55-65S, 850hPa for August 1 initialisation. Please see

402   text for details on how all of these quantities are defined. The year of 2002 is excluded from all

403   calculations. Bold values for AC - ERA indicate quantities that are statistically different from

404   zero at the 5% level based on a two-sided two-sample t-test.

Month	Signal (S)	Noise (N)	AC - S/N	AC - ERA	RMSE/Spread	RMSE/SD-ERA
Nov	1.45	1.34	0.74 (0.62, 0.83)	**0.71**	1.03 (0.83, 1.26)	0.71
Dec	1.12	2.12	0.47 (0.20, 0.65)	**0.46**	1.04 (0.83, 1.26)	0.89
Jan	0.71	1.96	0.34 (0.02, 0.55)	**0.37**	1.12 (0.83, 1.26)	0.93

405   **Table 3.**   As in Table 2, but for November 1 initialisation. Please note that hindcast AC values

406   in this table are not directly comparable with those in Figure 13b as here monthly means are

407   used rather than 7-day means.

[u] 55-65S Hindcast Correlation
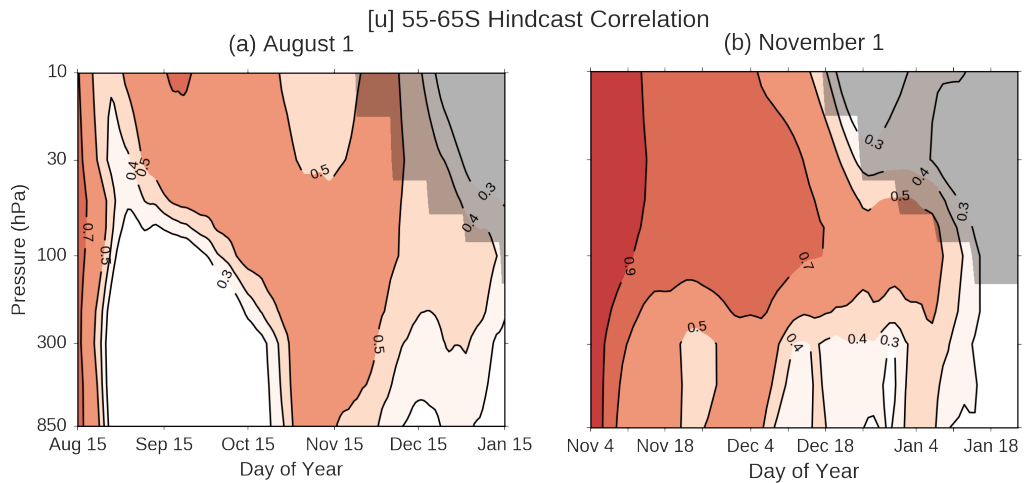
Figure 13. (a) Correlation between 31-day mean ensemble-mean [u] 55-65S and 31-day mean [u] 55-65S in ERA-Interim as a function of calendar day and pressure level for August 1 initialisation. Values on x-axis represent central date of 31-day mean. (b) As in (a), but for 7-day means for November 1 initialisation; note the expanded horizontal scale. In both figures all filled contour regions are statistically significant at the 5% level based on a two-sided two-sample t-test. Shaded area in top-right corner of each plot represents region where variability of [u] 55-65S becomes very small following SPV breakdown event. The year of 2002 is excluded from all calculations. Please note non-linear scale for contour intervals in the stratosphere.

tropospheric skill is seen to vanish following initialisation only to re-emerge again from October onwards. A similar result was previously found using a different set of hindcasts in *Seviour et al.* [2014]. As in that study, there is no evidence of a 'signal-to-noise' paradox, as all AC values are seen to fall within the 5-95% confidence interval of the expected AC from the hindcasts (Table 2 and Table 3).

As an alternative test of these conclusions, we compute the root-mean-square error of the ensemble-mean forecast (RMSE) and consider its ratio with the hindcast ensemble standard deviation about the ensemble mean (RMSE/Spread) and with the ERA-Interim interannual standard deviation (RMSE/SD-ERA; Table 2 and Table 3). For RMSE/Spread, a value less than one is an indicator of an over-dispersive hindcast ensemble and a value greater than one is an indicator of an under-dispersive ensemble. We have also included confidence intervals for RMSE/Spread; these were produced in a similar way to the confidence intervals for expected AC. Inspection of the results leads to the same conclusion as before: there is no evidence of an over-dispersive model ensemble (i.e., a 'signal-to-noise' paradox) for all months considered. Under these conditions, and under the assumptions of the general signal-to-noise model, the expected ratio RMSE/SD-ERA can be shown to equal $\frac{1}{(1+s^2)^{0.5}}$, where s is the signal-to-noise ratio. Hence the smaller the value, the more predictable is the state. We can see from Table 2 that there is evidence of a re-emergence of skill from October in the August 1 initialisations. Thus we conclude that there is evidence for tropospheric predictability on S2S timescales in austral spring and summer, and that there is no evidence of a signal-to-noise paradox between the hindcasts and reanalysis during this time.

Before summarising our results, we note that skilful forecasts of the EDJ may also indirectly act as a source of skill for other components of the climate system. As a particular example we highlight Antarctic sea-ice extent (Figure 14). During years where there is an early equatorward transition of the EDJ, summertime Antarctic sea-ice is seen to retreat more rapidly, with the opposite behaviour during years where there is a delay in the transition. It may also be possible to use such forecasts to infer behaviour about autumn Antarctic sea-ice extent, based on persistence of summertime SSTs [*Doddridge and Marshall*, 2018]. However, it should be cautioned that the seasonal retreat of Antarctic sea-ice is not restricted to the month of November alone [e.g., *Turner et al.*, 2017], and that November forecasts of the EDJ may only offer, at best, partial predictive power for summer and autumn Antarctic sea-ice extent.
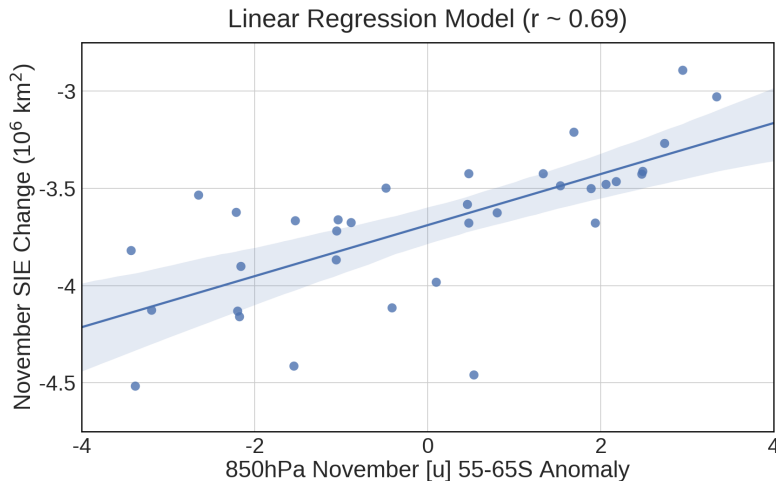
Figure 14. Linear regression between 850hPa November [u] 55-65S anomaly (m/s) and

November change in Antarctic sea-ice extent (km^2) from ERA-Interim and NSIDC, 1981-2015

(see Data and Methods section for further details). Shaded region represents 95% confidence

interval for regression line. The year of 2002 is excluded from the calculation.

5 Summary and Discussion

In this paper we have addressed specific issues of sampling variability and S2S pre-
dictability for the SH extratropical atmosphere by analysing a large ensemble of hind-
casts. Firstly, we have considered the impact of sampling variability on previous reanalysis-
based results for the relationship between the SPV, EDJ and ENSO. We have found that
coupled variability between the SPV and EDJ in the hindcast ensemble is in good agree-
ment with the reanalysis, and that this coupled variability is robust to sampling effects.
This coupled relationship between the SPV and the EDJ can be parsimoniously viewed
as a continuous shift of the entire seasonal cycle during austral spring and summer [*Byrne
and Shepherd*, 2018]. Moreover, the large sample size of the hindcast ensemble allows
the detection of nonlinearity in the SPV-EDJ relationship. We have also found that cou-
pled variability between ENSO and EDJ is robust to sampling variability but appears
to be via a stratospheric pathway, at least from August until the SPV breakdown event
sometime in austral summer. It should be noted that this result relates only to the high-
latitude zonally symmetric response to ENSO; it does not relate to any potential high-
latitude zonally asymmetric response.

Secondly, we have used the hindcast ensemble to show that shifts of the stratospheric seasonal cycle during this time of year can be expected to be predictable on S2S timescales, confirming what has been found in several previous studies. Following on from this result, we have introduced two statistical models of 'signal' and 'noise' for the troposphere, to estimate the predictable component of tropospheric variability associated with these predictable shifts of the stratospheric seasonal cycle. Both of these statistical models indicate that tropospheric predictability on S2S timescales is considerable between about mid-October and January. We have confirmed that the predictions of both of these signal/noise models are in good agreement with hindcasts that have been verified against a reanalysis. All of these results provide evidence of tropospheric predictability on S2S timescales from at least as early as August 1, and show no evidence of a 'signal-to-noise paradox' between the hindcasts and the reanalysis [*Scaife and Smith*, 2018]. We note that it may be the case that tropospheric predictability is larger in years with a more severe shift of the stratospheric seasonal cycle, with the SSW of 2002 perhaps the most extreme example of such behavior [see *Thompson et al.*, 2005, for a discussion of tropospheric impacts associated with the SSW of 2002.].

A potential future extension of our results relates to the early and mid-winter behavior of the SPV, when the SPV undergoes a poleward shift as part of its seasonal cycle [*Shiotani et al.*, 1993; *Kuroda and Kodera*, 1998]. The timing of this poleward shift is closely linked to the strength of the SPV during winter, and hence also to the strength of the SPV during spring and early summer [*Hio and Yoden*, 2005]. Thus it may be the case that skilful forecasts of the EDJ during spring and summer can be made from as early as June 1, based on knowledge of the timing of the poleward shift of the SPV during winter [*Lim et al.*, 2018]. Implicit in this statement is the assumption that a forecast model contains a realistic representation of the SPV seasonal cycle; given the broad spectrum of sub-gridscale parametrisations currently in use, this may not always be the case [*Polichtchouk et al.*, 2018].

References

Baldwin, M. P., and T. J. Dunkerton (2001), Stratospheric Harbingers of Anomalous Weather Regimes, *Science*, *294*(5542), 581–584, doi:10.1126/science.1063315.

Black, R. X., and B. A. McDaniel (2007), Interannual variability in the Southern Hemisphere circulation organized by stratospheric final warming events, *Journal of the Atmospheric Sciences*, *64*(8), 2968–2974, doi:10.1175/JAS3979.1.

Byrne, N. J., and T. G. Shepherd (2018), Seasonal Persistence of Circulation Anomalies in the Southern Hemisphere Stratosphere and Its Implications for the Troposphere, *Journal of Climate*, *31*(9), 3467–3483, doi:10.1175/JCLI-D-17-0557.1.

Byrne, N. J., T. G. Shepherd, T. Woollings, and R. A. Plumb (2017), Nonstationarity in Southern Hemisphere climate variability associated with the seasonal breakdown of the stratospheric polar vortex, *Journal of Climate*, *30*(18), 7125–7139, doi:10.1175/JCLI-D-17-0097.1.

Dee, D. P., S. M. Uppala, A. J. Simmons, P. Berrisford, P. Poli, S. Kobayashi, U. Andrae, M. A. Balmaseda, G. Balsamo, P. Bauer, P. Bechtold, A. C. M. Beljaars, L. van de Berg, J. Bidlot, N. Bormann, C. Delsol, R. Dragani, M. Fuentes, A. J. Geer, L. Haimberger, S. B. Healy, H. Hersbach, E. V. Hólm, L. Isaksen, P. Kållberg, M. Köhler, M. Matricardi, A. P. McNally, B. M. Monge-Sanz, J. J. Morcrette, B. K. Park, C. Peubey, P. de Rosnay, C. Tavolato, J. N. Thépaut, and F. Vitart (2011), The ERA-Interim reanalysis: Configuration and performance of the data assimilation system, *Quarterly Journal of the Royal Meteorological Society*, *137*(656), 553–597, doi:10.1002/qj.828.

Doddridge, E. W., and J. Marshall (2018), Modulation of the Seasonal Cycle of Antarctic Sea Ice Extent Related to the Southern Annular Mode, *Geophysical Research Letters*, *44*(19), 9761–9768.

Domeisen, D. I., C. I. Garfinkel, and A. H. Butler (2019), The Teleconnection of El Nino Southern Oscillation to the Stratosphere, *Reviews of Geophysics*, *57*, 5–47,

552   doi:10.1029/2018RG000596.

553   Gerber, E. P., M. P. Baldwin, H. Akiyoshi, J. Austin, S. Bekki, P. Braesicke,

554   N. Butchart, M. Chipperfield, M. Dameris, S. Dhomse, S. M. Frith, R. R.

555   Garcia, H. Garny, A. Gettelman, S. C. Hardiman, A. Karpechko, M. Marc-

556   hand, O. Morgenstern, J. E. Nielsen, S. Pawson, T. Peter, D. A. Plummer,

557   J. A. Pyle, E. Rozanov, J. F. Scinocca, T. G. Shepherd, and D. Smale (2010),

558   Stratosphere-troposphere coupling and annular mode variability in chemistry-

559   climate models, *Journal of Geophysical Research: Atmospheres*, *115*(D00M06),

560   doi:10.1029/2009JD013770.

561   Hio, Y., and S. Yoden (2005), Interannual variations of the seasonal march in the

562   Southern Hemisphere stratosphere for 1979 - 2002 and characterization of the

563   unprecedented year 2002, *Journal of the Atmospheric Sciences*, *62*(3), 567–580,

564   doi:10.1175/JAS-3333.1.

565   Hitchcock, P., and I. R. Simpson (2014), The Downward Influence of Stratospheric

566   Sudden Warmings, *Journal of the Atmospheric Sciences*, *71*(10), 3856–3876, doi:

567   10.1175/JAS-D-14-0012.1.

568   Hurwitz, M. M., P. A. Newman, L. D. Oman, and A. M. Molod (2011), Response

569   of the Antarctic Stratosphere to Two Types of El Nino Events, *Journal of the*

570   *Atmospheric Sciences*, *68*(4), 812–822, doi:10.1175/2011JAS3606.1.

571   Kumar, A. (2009), Finite Samples and Uncertainty Estimates for Skill Measures for

572   Seasonal Prediction, *Monthly Weather Review*, *137*(8), 2622–2631.

573   Kuroda, Y., and K. Kodera (1998), Interannual variability in the troposphere and

574   stratosphere of the Southern Hemisphere winter, *Journal of Geophysical Research*,

575   *103*(D12), 13,787, doi:10.1029/98JD01042.

576   L'Heureux, M. L., and D. W. J. Thompson (2006), Observed Relationships between

577   the El Nino-Southern Oscillation and the Extratropical Zonal-Mean Circulation,

578   *Journal of Climate*, *19*(2), 276–287, doi:10.1175/JCLI3617.1.

579   Lim, E.-P., H. H. Hendon, and H. Rashid (2013), Seasonal Predictability of the

580   Southern Annular Mode due to Its Association with ENSO, *Journal of Climate*,

581   *26*(20), 8037–8054.

582   Lim, E.-P., H. H. Hendon, and D. W. J. Thompson (2018), Seasonal Evolution of

583   Stratosphere-Troposphere Coupling in the Southern Hemisphere and Implica-

584   tions for the Predictability of Surface Climate, *Journal of Geophysical Research:*

Atmospheres, *123*(21), 12,002–12,016, doi:10.1029/2018JD029321.

Lin, P., Q. Fu, and D. L. Hartmann (2012), Impact of Tropical SST on Stratospheric Planetary Waves in the Southern Hemisphere, *Journal of Climate*, *25*(14), 5030–5046, doi:10.1175/JCLI-D-11-00378.1.

Molteni, F., T. Stockdale, M. A. Balmaseda, G. Balsamo, R. Buizza, L. Ferranti, L. Magnusson, K. Mogensen, T. N. Palmer, and F. Vitart (2011), *The new ECMWF seasonal forecast system (System 4)*, 656, ECMWF, Reading, UK.

Polichtchouk, I., T. G. Shepherd, and N. J. Byrne (2018), Impact of Parametrized Nonorographic Gravity Wave Drag on Stratosphere-Troposphere Coupling in the Northern and Southern Hemispheres, *Geophysical Research Letters*, *45*(16), 8612–8618, doi:10.1029/2018GL078981.

Polvani, L. M., L. Sun, A. H. Butler, J. H. Richter, and C. Deser (2017), Distinguishing Stratospheric Sudden Warmings from ENSO as Key Drivers of Wintertime Climate Variability over the North Atlantic and Eurasia, *Journal of Climate*, *30*(6), 1959–1969, doi:10.1175/JCLI-D-16-0277.1.

Roff, G., D. W. J. Thompson, and H. Hendon (2011), Does increasing model stratospheric resolution improve extended-range forecast skill?, *Geophysical Research Letters*, *38*(5), doi:10.1029/2010GL046515.

Roscoe, H. K., J. D. Shanklin, and S. R. Colwell (2005), Has the Antarctic vortex split before 2002?, *Journal of the Atmospheric Sciences*, *62*(3), 581–588, doi:10.1175/JAS-3331.1.

Scaife, A. A., and D. Smith (2018), A signal-to-noise paradox in climate science, *npj Climate and Atmospheric Science*, *1*(1), 28, doi:10.1038/s41612-018-0038-4.

Seager, R., N. Harnik, Y. Kushnir, W. Robinson, and J. Miller (2003), Mechanisms of Hemispherically Symmetric Climate Variability, *Journal of Climate*, *16*(18), 2960–2978, doi:10.1175/1520-0442(2003)016¡2960:MOHSCV¿2.0.CO;2.

Seviour, W. J. M., S. C. Hardiman, L. J. Gray, N. Butchart, C. MacLachlan, and A. A. Scaife (2014), Skillful seasonal prediction of the Southern Annular Mode and Antarctic ozone, *Journal of Climate*, *27*(19), 7462–7474, doi:10.1175/JCLI-D-14-00264.1.

Shiotani, M., N. Shimoda, and I. Hirota (1993), Interannual variability of the stratospheric circulation in the Southern Hemisphere, *Quarterly Journal of the Royal Meteorological Society*, *119*(511), 531–546.

618 Sigmond, M., J. F. Scinocca, V. V. Kharin, and T. G. Shepherd (2013), Enhanced

619   seasonal forecast skill following stratospheric sudden warmings, *Nature Geo-*

620   *science*, *6*, 98–102, doi:10.1038/ngeo1698.

621 Son, S. W., A. Purich, H. H. Hendon, B. M. Kim, and L. M. Polvani (2013), Im-

622   proved seasonal forecast using ozone hole variability?, *Geophysical Research Let-*

623   *ters*, *40*(23), 6231–6235, doi:10.1002/2013GL057731.

624 Son, S.-W., B.-R. Han, C. Garfinkel, S.-Y. Kim, R. Park, N. Abraham, H. Akiyoshi,

625   A. Archibald, N. Butchart, M. Chipperfield, M. Dameris, M. Deushi, S. Dhomse,

626   S. Hardiman, P. Joeckel, D. Kinnison, M. Michou, O. Morgenstern, F. O'Connor,

627   L. Oman, D. Plummer, A. Pozzer, L. Revell, E. Rozanov, A. Stenke, K. Stone,

628   S. Tilmes, Y. Yamashita, and G. Zeng (2018), Tropospheric jet response to

629   Antarctic ozone depletion: An update with Chemistry-Climate Model Initiative

630   (CCMI) models, *Environmental Research Letters*, *13*(5).

631 Sun, L., G. Chen, and W. A. Robinson (2014), The role of stratospheric polar vortex

632   breakdown in Southern Hemisphere climate trends, *Journal of the Atmospheric*

633   *Sciences*, *71*(7), 2335–2353, doi:10.1175/JAS-D-13-0290.1.

634 Thompson, D. W., M. Baldwin, and S. Solomon (2005), Stratosphere-troposphere

635   coupling in the Southern Hemisphere, *Journal of Atmospheric Sciences*, *62*, 708–

636   715.

637 Turner, J., T. Phillips, G. J. Marshall, J. S. Hosking, J. O. Pope, T. J. Bracegirdle,

638   and P. Deb (2017), Unprecedented springtime retreat of Antarctic sea ice in 2016,

639   *Geophysical Research Letters*, *44*(13), 6868–6875.

640 van Loon, H. (1967), The half-yearly oscillations in middle and high southern lati-

641   tudes and the coreless winter, *Journal of the Atmospheric Sciences*, *24*, 472–486,

642   doi:10.1175/1520-0469(1967)024¡0472:THYOIM¿2.0.CO;2.

643 Vera, C. S., and M. Osman (2018), Activity of the Southern Annular Mode during

644   2015-2016 El Nino event and its impact on Southern Hemisphere climate anoma-

645   lies, *International Journal of Climatology*, *38*(S1), 1288–1295.

646 Weisheimer, A., D. Decremer, D. MacLeod, C. O'Reilly, T. Stockdale, S. Johnson,

647   and T. Palmer (2019), How confident are predictability estimates of the winter

648   North Atlantic Oscillation?, *Quarterly Journal of the Royal Meteorological Society*,

649   *0*(0), doi:10.1002/qj.3446.

650   White, C. J., H. Carlsen, A. W. Robertson, R. J. Klein, J. K. Lazo, A. Kumar,

651   F. Vitart, E. Coughlan de Perez, A. J. Ray, V. Murray, S. Bharwani, D. MacLeod,

652   R. James, L. Fleming, A. P. Morse, B. Eggen, R. Graham, E. Kjellström,

653   E. Becker, K. V. Pegion, N. J. Holbrook, D. McEvoy, M. Depledge, S. Perkins-

654   Kirkpatrick, T. J. Brown, R. Street, L. Jones, T. A. Remenyi, I. Hodgson-

655   Johnston, C. Buontempo, R. Lamb, H. Meinke, B. Arheimer, and S. E. Zebiak

656   (2017), Potential applications of subseasonal-to-seasonal (S2S) predictions, *Meteo-*

657   *rological Applications*, *24* (3), 315–325.

658   WMO (2013), Subseasonal-to-seasonal prediction: research implementation

659   plan, *Tech. rep.*, WMO, https://library.wmo.int/pmb_ged/2014_wcrp_sub-

660   seasonal_to_seasonal_prediction_en.pdf.

661   Zubiaurre, I., and N. Calvo (2012), The El Nino-Southern Oscillation (ENSO)

662   Modoki signal in the stratosphere, *Journal of Geophysical Research: Atmospheres*,

663   *117*(D4), doi:10.1029/2011JD016690.